SLAC-PUB-3043
CERN TIS-RP/100/PP
January 1983
(I/A)

TRANSPORT OF HIGH ENERGY MUONS IN A SOIL SHIELD*

WALTER R. NELSON AND THEODORE M. JENKINS
Stanford Linear Accelerator Center
Stanford University, Stanford, California 94305

GRAHAM R. STEVENSON, MAGNUS NIELSEN,
ERIK H. M. HEIJNE AND PIERRE JARRON
CERN, Geneva, Switzerland

JERE LORD AND STEVEN ANDERSON†
University of Washington, Seattle, Washington

ABSTRACT

An experiment is described in which measurements were made of the fluence of muons as a function of radial distance at a depth of about 350 meters in a soil shield irradiated by a beam of muons at 200, 240 and 280 GeV/c. Three measurement techniques were employed: a scintillator telescope, a semiconductor detector telescope, and nuclear emulsions. The data recorded by the different techniques show agreement among themselves. They are compared with transport calculations based on the Fermi-Eyges model and on Monte Carlo calculations. The differences between the observed data and the calculations are discussed, but there is general agreement between data and calculations to better than a factor of two over a range of four orders of magnitude in fluence per incident muon.

Submitted to Nuclear Instruments and Methods

---

* Work supported by the Department of Energy, contract DE-AC03-76SF00515.

† Work supported by the Department of Energy, contract DE-AC06-81ER40048.

1. INTRODUCTION

In the shielding of high energy accelerators, muons can be the dominant source of penetrating radiation. Muons easily penetrate massive shields, a direct result of their weakly interacting nature, as is clearly shown in the range-energy curves of fig. 1 [1]. At electron accelerators, muons are created mainly from pair production, while the dominant mechanism at proton accelerators is pion or kaon decay. For both accelerators, muons are produced primarily in the forward direction, and thus the shielding is much more extensive around beam dumps and targets in the beam direction. This is not to imply that the transverse shielding problem is negligible for muons. On the contrary, experiments at SLAC have shown muon contributions at relatively wide angles [2], while a prompt muon (as opposed to the more common pi-mu decay) component has been observed in proton accelerator experiments (see, for example, [3]). These prompt muons will contribute to muon doses at large angles at high proton energies. Furthermore, at muon energies above 10 GeV, interaction mechanisms other than ionization and excitation begin to contribute to the slowing down and scattering of muons [4]. This leads to two effects: 1) the range of the muon is shortened, and 2) the additional decrease in muon energy along the path of the muon and the scattering due to these inelastic events themselves result in an increase in the lateral spread of the beam.

There have been many theoretical studies of the production and transport of muons at proton accelerators [5-11], but apart from a preliminary report on the initial phase of this experiment [12], no experimental verification of the theoretical methods has been reported to date. This is especially unfortunate because there is evidence to suggest there may be significant discrepancies between calculations and measurements, at least at an electron accelerator. One measurement and a comprehensive theoretical study of the production and transport of muons around electron accelerators have been published [2,13,14], where a larger-than-predicted wide angle muon fluence was found in the measurements.

The problem of multiple scattering with slowing down in a shield can be solved analytically using the model of Eyges [15], as in the analytic computer code, TOMCAT [16], or using Monte Carlo techniques as in the muon section of the hadronic cascade code, CASIM [10,17]. Coulomb, nuclear and bremsstrahlung scattering processes are all taken into account. In fact, if a code is up to date, then all processes which can alter the

diffusion profiles in any significant way can be taken into account, such as, for example, range straggling.

An experiment designed to study only the transport part of the muon shielding problem, exclusive of the source term, would aid in the understanding of the SLAC muon measurements, as well as provide a true quantitative test of the computational methods currently being employed around both types of accelerators. In addition, the experimental data should be of direct use in studies of the attenuation of cosmic ray muons in earth.

Accurate computation of the lateral diffusion of muon beams is also important in the prediction of off-site radiation levels at high energy accelerators [18,19]. It was to check out transport programs such as TOMCAT that the present experiment was designed.

The measurements presented here were made in the North Experimental Area at CERN during the period from January 1979 through June 1980 using muons in the momentum range between 200 and 280 GeV/c. The muon beam at this facility is ideal because the beam is monoenergetic, small in cross sectional area, has little angular divergence relative to the spread caused by multiple scattering in the shield, and the incident intensity and other parameters are well known. In addition, the earth backstop is composed of undisturbed soil and therefore can be considered to be fairly homogeneous.

The following sections will describe in detail the experiment and give results. The experimental geometry will be covered first in sect. 2, along with some of the general items associated with the experiment (such as muon intensities, beam triggers, etc.). Next, sect. 3 will describe the various detector systems that were used. Theoretical models and the computer codes that were used in this study will be described in sect. 4. Section 5 will describe the types of measurements and the results, where comparisons are made with experimental data. The last part (sect. 6) summarizes the findings and discusses the implications of this work.

2. EXPERIMENTAL SETUP

The external muon beam (M2) in the North Area of CERN passes through a building (EHN2) which at the time of these measurements contained two large experiments, designated NA2 and NA4, prior to entering a soil backstop (see figs. 2, 3). The backstop and the area further downbeam are part of a quiet rural countryside, although contained

within the CERN boundary fences. This area was predetermined to be ideal for a muon transport experiment because the soil shield itself had not previously been excavated and also, background radiation levels from surrounding experiments were considered to be negligible; that is, only one other experimental area, EHN1 (not shown), was operational 500 m upbeam and 80 m to the side of EHN2. The density of the earth in this area was measured to be between 1.9 and 2.1 g/cm^3.

Muon beam intensities passing through EHN2 were of the order of $1.5 \times 10^7 \mu/pulse$ (1 sec pulse width at 6 ppm), as measured with charge collecting ion chambers, and were known to about 1-2% uncertainty. Momenta were analysed to an uncertainty of less than 10%.

At a location 292 meters downbeam of the start of the soil backstop behind EHN2, two 40 cm diameter holes were drilled vertically into the ground and lined with plastic pipes which were closed at the bottom to prevent water seepage. One of the holes was aligned with the theoretical beam centerline projected through the backstop from the NA2/NA4 experiments, and the other was located at a distance of 3.94 meters (center-to-center) on a line normal to this beam centerline. Each hole extended a total distance of 5 meters into the ground such that the plane of the beam axis was about 1.5 meters above the bottom of the holes. The plastic pipes projected above the earth surface about one meter as shown in fig. 4.

As described in more detail in the next section, three types of detectors were used to measure muon fluences in the holes: scintillation counters, nuclear track emulsions and silicon detectors. In order to allow for reasonably accurate positioning of these detectors, an aluminum I-beam was installed in each pipe as shown in fig. 5. Both I-beams were fixed to the sides of the pipes with their flat surfaces aligned parallel to the theoretical beam axis.

The electronic detectors were attached to platforms which rolled on the inside of the I-beams, their vertical position held in place by a metal chain which was scaled relative to a fixed position near the top of the hole, and therefore, to the beam centerline. It was anticipated that many of the emulsion exposures would have to be initiated with the muon beam already on, requiring that they be lowered quickly to fixed positions. This was accomplished by placing them on small supports attached to 1.5 meter long aliminum plates which slid adjacent to the I-beams by means of teflon slides riding in the

inside of the I-beams. A total of four aluminum plates, stacked one on top of another for a total vertical distance of 6 meters, was used in each hole. Each of the small L-bracket supports for the emulsions could be aligned either perpendicular or parallel to the beam axis.

A bending magnet, (B9), located just downstream of the carbon target in EHN2 and normally kept on by the NA4 experiment, was turned off during the emulsion exposures or when counter data were being taken. However, most of the preliminary counter checkout was performed in the off-axis hole with B9 turned on to a nominal setting since the beam axis in this case was shifted to within one meter of the center of this hole. The electronics associated with the various detectors were housed inside a small hut located adjacent to the holes. A trigger signal from the accelerator extraction was delivered by cable such that background and detector noise could be reduced by gating techniques. During periods of measurement, the intensity of the muon beam, as well as vertical and horizontal profiles measured with multiwire proportional chambers before and after the NA4 experimental setup, were recorded.

3. DESCRIPTION OF DETECTORS

Three detector systems were used, each of which allowed for an independent measurement of the radial distribution of muon fluence in the hole. Also, each gave some extra information that the others did not, such as angular information for the emulsions, etc. The three detector systems were 1) scintillation counters, 2) nuclear emulsions and 3) a silicon diode telescope. The scintillation counters provided a quick and dependable measurement of the radial fluence profile. As fixed counters, they were left on and allowed to integrate during each of the emulsion exposures and provided information related to changes in beam conditions (i.e., steering, divergence, etc.).

The nuclear emulsions were exposed both parallel as well as perpendicular to the general direction of the muon beam. In addition to a check on the counter measurements, emulsions gave information about the angular distribution of the tracks and possibly some indication as to whether or not hadrons, electrons or photons accompanied the muons in the shield. Emulsion exposures were also made in the EHN2 building in order to provide angular distributions of the incident beam to complement the spatial distri-

butions provided by the beam profile monitors associated with the NA2/NA4 experiments.

A small silicon diode telescope was used in order to determine the extent, if any, of muon initiated electromagnetic cascades accompanying the muon field [20,21].

3.1 Scintillation Counters

Four scintillation counters were used in the experiment. Two, CA and CB, were combined to form a telescope that could traverse the vertical limits of either hole, and the others, R1 and R2, were fixed at the bottom of hole 1 (on-axis) and hole 2 (off-axis), respectively. The fixed counters were used as reference counters to record changes in the incident beam intensity and/or angular distribution. Each counter consisted of a 1 cm thick NE102 plastic scintillator optically coupled to an Amperex 56AVP photomultiplier tube. The scintillators in the fixed counters were 5 cm in width and 20 cm in height, and were oriented such that the area was normal to the theoretical beam axis. The movable telescope , also oriented perpendicular to the beam direction, consisted of a 3 cm by 3 cm scintillator, CA, centered in front of a 14 cm wide by 20 cm high scintillator, CB. Separation distance between the two was 20 cm. When used in coincidence, they effectively formed a coarse ($\simeq 30^o$) telescope pointing back to the source.

Signals from the counters were processed using standard NIM electronics as shown schematically in fig. 6. The counter plateaus were determined with one counter positioned on beam axis in the central hole, and the others used as beam monitors. The absolute efficiency of each counter was not determined, but is assumed to be at least 95%. The telescope timing and the plateaus were rechecked at the start of each series of runs, and the high voltages monitored throughout the entire experiment. No significant changes were noted.

3.2 Nuclear Track Emulsions

Two groups of emulsions were used, one a typically thick (400 μ) set poured onto 1 by 3 inch glass plates using either Ilford or Kodak emulsion, and a second group composed of a 500 μ thick metacryl plastic with 80 μ thick Fuji emulsion poured onto each side as depicted in fig. 7. This geometry had been used previously [22] for 10 GeV muons and 18 GeV electrons with relative angles measureable to a precision of 0.1 mradians. The thicker emulsions were placed with their long axes parallel to the beam, and were intended primarily to determine the hadron fluence (if any) accompanying the

muons. In addition, they provided a backup to fluence data measured with the double-coated plates. Because of the movement of the emulsion with time and temperature, precise angular information is not possible from the thicker emulsions. More precise angular information is possible from the double-coated plastic since only the entry and exit points at the emulsion/plastic interface need to be measured in order to determine the angle through the 500 μ thick plastic. Even though the plate orientation was not established to better than a few degrees to the beam direction, it was anticipated that relative angles would be measureable to a precision of better than 0.5 milliradians using this technique.

Eight double-coated plates were prepared using the Fuji photographic emulsion gel. The plates were prepared in Seattle during the period 1-6 May, 1980, and ranged in size from 10 cm by 15 cm to 20 cm by 25 cm prior to being cut into smaller sizes for exposure.

The plates accumulated from 5 to 25 days of sea level-to-CERN altitude exposure, and about 10 hours of exposure at about 10,000 meters. This corresponds to between 8000 and 20,000 minimum ionizing tracks/cm^2-sr of background. The plates were always oriented perpendicular to the vertical, and the background tracks on the plates are given from the $cos^2\theta$ angular distribution of cosmic ray particles (relative to the vertical).

Seven separate exposures were made in three different momenta at five different exposure sites. The sites were upstream and downstream of the carbon target of the NA4 experimental area, and at relative vertical positions 465, 247 and 67 cm in the on-axis hole. (The relative vertical distance to the beam centerline was determined by survey to be 454.6 cm.) In addition, background emulsions were placed on the fence 50 meters lateral to the experiment as well as back in the darkroom.

3.3 Silicon Diode Measurement

A small silicon diode telescope (referred to as the "tiny" telescope), originally designed to measure flux profiles of high intensity muons with electron rejection [20,21], was also included. Using the coincidence between a small area front diode and a larger area rear detector, the differences between signals with and without lead between the detectors can be a measure of the electron contamination in the muon beam. This is due to the electromagnetic shower that is developed in a material (such as lead) from high energy electrons, but which is not present when muons traverse the same material.

Four silicon detectors, 41,42,61 and 62, with surface areas ranging from 0.26 to 2.0 cm^2, were positioned relative to one another to form what we refer to as the "long" telescope (fig. 8). In addition to this arrangement, the upstream pair (41 and 42), with 6 mm of lead between them, constituted the "tiny" telescope that was used to make fluence measurements in the on-axis hole. The detectors were connected to a fast voltage sensitive preamplifier which drove a 20 m long coaxial cable. The low counting rates in this experiment permitted the use of a standard main amplifier with a pulse shaping time constant of 1 μsec. The upstream detector signal was fed into a pulse height analyzer and was also counted in a 100 MHz scaler provided that the signal arrived in coincidence with a signal from the second, slightly larger, diode in either telescope arrangement.

4. THEORETICAL MUON TRANSPORT CODES

Two different muon transport codes were used, one a Monte Carlo transport code, TRANMU, adapted from the larger hadronic transport code, CASIM [10], and the second the analytic code, TOMCAT [16].

TRANMU employs the continuous slowing-down approximation. The range-energy relation includes effects of ionization, bremsstrahlung, pair-production and nuclear interaction. Multiple scattering of the muons is calculated by the Monte Carlo method. Coulomb scattering is treated by the Gaussian approximation [23]. For muons above 10 GeV, contributions to the scattering due to bremsstrahlung and nuclear interactions become appreciable and are included. Contributions to the scattering from pair production are assumed to be negligible at all energies. The angular distribution due to multiple bremsstrahlung and nuclear interaction are likewise assumed to be Gaussian with a mean square distance as calculated by Alsmiller [6].

TOMCAT solves the muon transport analytically even though the incident muon parameters may be determined by Monte Carlo methods. It uses the Fermi-Eyges theory [15, 24] in which all range straggling is ignored and the range-momentum relationship is assumed to be monotonic. In addition, all scattering is considered to be the sum of many individual small-angle scattering processes. Coulomb scattering from the nuclei of atoms, and to a lesser extent from orbital electrons, bremsstrahlung production from muon-nucleus collisions, and muon-nucleus non-elastic collisions are all taken into account

when determining the mean square angle of scattering per unit distance. Empirical formulae of the form

$$\chi^2 = \alpha E^{-\beta} \ ,$$

where E is the muon energy, have been fitted to the variation of the mean square scattering angle, χ^2, as a function of muon energy as calculated by Alsmiller [6] for each of the Coulomb, nuclear and bremsstrahlung scattering processes. Pair-production from muon-nucleus collisions is assumed to be small and is ignored. The continuous slowing-down approximation for muons is used in TOMCAT, i.e., straggling is ignored, single large energy loss processes are averaged and a single value of the range is assumed for any momentum value.

Both codes were run for the geometry shown in fig. 3 for each of the energies used in this experiment. The results, given in figs. 9-12, show essential agreement between the two codes. TOMCAT is very much faster than TRANMU, although the latter is capable of providing additional information (i.e., angular and energy distributions). Because the two codes agree, the experimental results, except for angular measurements, will henceforth be compared only with TOMCAT.

5. MEASUREMENTS AND RESULTS

(a) Scintillator

The input muon beam had a slight momentum spread and an inherent radial-angular distribution that was further perturbed by the carbon target in the NA4 experiment (see fig. 3).

Figure 13 shows the muon fluence at various radial positions (i.e., relative vertical distances) as measured with the scintillators at 280 GeV/c. The off-axis (Hole 2) data were plotted using an "effective" vertical distance, assuming knowledge of the beam centerline. Unless indicated otherwise, the error bars are the size of the symbols themselves. Also shown is the TOMCAT calculation. The scintillator data for 240 and 200 GeV/c with the carbon target in place are shown in figs. 14 and 15. Several features can be noted at once.

1. At 280 and 240 GeV/c, TOMCAT agrees reasonably well with measurements over several decades, especially in view of the fact that no normalization has been made to the data.

2. For all three momenta, the tail of the distribution appears to flatten out somewhat. As indicated in the figures, this occurs near the earth-air interface, suggesting that a background source is becoming important. However, some of the points to the right of the earth-air line correspond to measurements made deep inside the off-axis hole. It is apparent that the measurements in this 'tail' region still are significantly above the TOMCAT curves for both the 280 and 240 GeV/c runs.

3. The data appear to be symmetric about the surveyed beam centerline, as expected.

4. At 280 GeV/c, and to a lesser extent at 240 GeV/c, there appear to be too many particles around the beam centerline.

5. At 200 GeV/c (fig. 15), TOMCAT no longer agrees with measured data.

The last item might be explained by straggling effects that are not correctly accounted for in either TOMCAT or TRANMU. One way of checking this would be to remove a part of the shield. This was accomplished by removing the 50 m carbon target inside building EHN2. The measurements at 200 GeV/c with this geometry are shown in fig. 16. The agreement with TOMCAT again appears more reasonable.

As a further check on this presumed straggling effect, the total fraction of muons under the curves in figs. 13-16 were obtained by numerical fitting and integration techniques. The results are given in table I where unity would be expected if no particles were either lost or produced in the shield. The same numerical techniques were employed on both the TOMCAT and TRANMU results for all conditions, with a resulting fraction of 1.0, as expected.

It is apparent that a significant fraction (67%) of the incident muons never reach the detector plane at 200 GeV/c. The removal of a portion of the shield (i.e., 50 m carbon target) allows more of the muons to reach the detectors, although 12($\pm$ 3)% are still not accounted for. Calculations of muon straggling in soil [25] suggest that whereas 92% of incident muons should reach the detectors for the 200 GeV/c (no carbon) case, in agreement with the experimental data, 83% should still reach the detector in the

200 GeV/c (with carbon target) case. This is in conflict with the data; however, these straggling calculations did not allow for multiple scattering.

We also note from table I that there appear to be too many particles at the higher momenta, particularly at 280 GeV/c. This is consistent with the discrepancy around the beam centerline seen in figs. 13 and 14, and noted above. While the absolute disagreement may be subject to criticism due to the uncertainties, the trend seems to be real. There are too many 'apparent' muons as the energy increases, which may be explained as being due to processes not accounted for in the computer codes, such as energetic delta rays produced by muons and leading to electromagnetic cascades.

(b) Emulsion

Although two types of emulsion were exposed, it was sufficient to scan only the double-coated plates in order to obtain the results presented here.

Due to the lack of thermal equilibrium on the microscope viewing stage, together with the relatively large separation of the two metacryl surfaces, the noise in measuring the fiducial direction was found to be larger than the signal being measured. In a series of measurements on the same set of tracks carried out over a six hour period, there was a random drift of the fiducial direction that had a maximum excursion of about 13 mradians (rate of drift $\simeq$ 4 mrads per hour). Measurements of tracks with respect to a given fiducial repeated in less than 5 minutes were reproducible to about 0.7 mrads. As a result, the perpendicular to the metacryl surface, the fiducial direction (defined by the vertical microscope stage movement down through the metacryl), cannot be used as an absolute reference axis throughout a given plate, since the tracks have angles on the order of 5 to 15 mrads. Anticipating this, the emulsions were not precisely aligned to better than a few degrees with respect to the beam direction.

The following method was therefore employed. A group of 12 tracks which could be identified by pattern on both the upper and lower emulsion-metacryl surface was selected. Within a short time span, the coordinates on both surfaces were determined for each of the twelve tracks. An inclusive method of determining root-mean-square angles was then employed.

Angular measurements were made only for the 280 GeV/c case at the relative vertical distance of 465 cm (i.e., about 10 cm from the beam centerline). A total of 9 groups of about 12 tracks each were measured, for a total of 106 actual tracks. However, 9 tracks

(one from each group) were not considered in the angular measurements since they were used to determine the perpendiculars, so that 97 tracks in all were used.

The computer code, TRANMU, was then run for the same general geometry, also at 280 GeV/c, and the data scanned for a radius of 20 cm from the beam centerline. The results from the emulsion data and TRANMU are shown in fig. 17. The measurement data are broader than the calculated data, but in view of the method that was employed, not too much emphasis should be placed on the differences. What should be noted is that the angles are quite small.

Fluences were obtained from similar scans over a sample area of 10^4 μm^2 for all three momenta. An angular cut-off of 5^o with respect to the vertical to the emulsion surface was used. The results are plotted on an absolute basis in figs. 18-20. The data are in good agreement with the scintillator measurements (shaded bands) off the beam axis. The emulsion points along the beam centerline appear to lie between the counter data and TOMCAT curves at the higher momenta. Because the emulsion scanning is biased toward selection of tracks at small angles ($< 5^o$), this observation is not surprising.

The scintillators respond to tracks at all angles (singles), and to tracks with angles less than 30^o (coincidence). Since the coincidence-to-single ratio was measured to be 97% in the forward direction at 280 GeV/c, the difference between the counter and emulsion data might be due to tracks between 5 and 30^o. A possible explanation, as previously given, might be very energetic knock-on electrons or even their subsequent showers.

(c) Silicon Diodes

As described earlier, a "tiny" silicon diode telescope was used to measure the fluence in the on-axis hole at 280 GeV/c. The results are presented in fig. 21, where the absolute fluence is in reasonabale agreement with the scintillator data, but is systematically higher than the TOMCAT curve.

Additional measurements were made at 280 GeV/c using the "long" telescope arrangement (see fig. 8) in an attempt to determine if electrons are present in significant numbers along with the muons. The "long" telescope was positioned between two 5 $\times$ 20 cm^2 scintillators at a relative vertical position of 450 cm in the on-axis hole. The results are given in table II where S1 and S2 refer to the upstream and downstream scintillators respectively, and 41, 42, 61, and 62 are the silicon diodes as shown in fig.

8. Three measurements are given in the table, corresponding to the orientation of the "long" telescope between the scintillators; namely, 41 upstream and 62 downstream (A), reversed orientation (B), and original orientation repeated (A′). The data have been normalized to S1. Both single and coincidence data are presented.

It becomes clear that reversing the telescope has an important effect on the count rate in the single detectors. The smallest upstream detector, 41, changes most, the biggest 2 cm^2 detector, 61, changes the least. The idea that the higher counting rate is caused by individual electrons is at least qualitatively suggested by this test. From table II it can also be noted that the ratio between the small silicon detectors and the $20 \times 5cm^2$ scintillators is not constant (i.e., compare runs A and A′) to more than 10-15%. This can be explained in part by changes in the relative position of the telescope or variations in the beam. This is not inconsistent with the variation in the scintillator data by itself, as suggested by the "bands" in our figures.

(d) B9 Measurements

The radial profile was also determined at 200 GeV/c by horizontally sweeping magnet B9 and measuring the fluences in both the on-axis and off-axis holes using scintillators. This method avoids the problems associated with the earth-air interface since, in this case, the detectors remain fixed vertically well down inside the holes while the horizontal beam direction only is varied. The on-axis counter, CB, was positioned on the beam centerline, while the off-axis counter, R2, was 82.9 cm below the plane of the beam. The results are shown in fig. 22 where good agreement with the other scintillator telescope data (shaded band) can be seen.

6. SUMMARY AND CONCLUSIONS

This experiment was initiated by selecting a site at CERN that had 1) a pure muon beam already momentum analyzed, and 2) a well-defined homogenous soil shield. The locations in the shield in which to make the measurements were chosen to be near the end of the muon range for 200 GeV/c muons, and upstream of the end-of-range for the higher momenta. The holes were dug deep enough to include (theoretically, at least) three or more orders of magnitude change in muon intensity. Background problems and perhaps problems due to the lack of soil in the upper regions (where the air exists) were anticipated, but it was hoped that the effect of these would not be too great. It was also

anticipated that data from deep inside the off-axis hole would supplement and clarify the wide angle data taken near or above the earth-air interface from the on-axis hole.

In fact, the region near and above the earth-air interface gives data at the wider angles which are above the calculated levels (i.e., at the relative distances of less than 100 cm which corresponds to about 9 mradians). The data from the second (off-axis) hole, scanty for all momenta except 280 GeV/c, are lower than the on-axis data taken near or above the earth-air interface, but are still substantially above the theoretical curve at these relatively wide angles. Sweeping the beam horizontally with magnet B9 essentially confirms the data taken vertically, but this set of data was taken only at 200 GeV/c where the tail is already ill-defined.

The comparison between measurement and calculation certainly is as interesting in the forward direction, but again is not well understood. Specifically, it would appear that there are too many particles in the forward direction for the higher momenta (280 and 240 GeV/c) and too few for the 200 GeV/c momentum. This seems to be a function of momentum, i.e., higher momentum gives more particles, and this is further confirmed by the silicon diode fluence measurements at 280 GeV/c. The case of too few particles in the forward direction continues at 200 GeV/c even when some of the shield is removed, though to a lesser extent.

Integrating the total number of particles under the curves confirms that the higher than expected fluence in the forward direction is caused by an excess of particles at the higher momenta. It is postulated that many, and perhaps, most of these are from very energetic knock-on electrons and subsequent electromagnetic cascades. Neither the emulsion nor the silicon diode data were able to confirm this, but both gave answers that were in the right direction.

The most obvious discrepancy between theory and measurement is the very much lower fluence near the end-of-range. The present codes fail badly in this region. It can be argued that for most purposes (i.e., shielding), this region is relatively unimportant. Apart from this anomaly, it can be concluded that current muon transport codes are capable of predicting fluence radial profiles in soil to within a factor of two over 4 orders of magnitude.

ACKNOWLEDGEMENTS

We wish to thank the CERN laboratory for making the facilities available for this experiment and for providing travel assistance for one of the authors (TMJ) and a visiting scientist position for another (WRN). We have been fortunate to have received help from and are grateful to several groups and individuals, among which are: J. May and E. Rossa of EP and SPS Divisions, respectively; J. Feltese, E. Gabathuler, R. Kopp, C. Rubbia, D. Schinzel, and C. Zupancic of the NA2 and NA4 experiments; E. Mendola and G. Vanderhaeghe who provided us with the darkroom facilities; A. Van Ginneken (FNAL) for help in using the muon subprogram of CASIM; H. DeStaebler (SLAC) for many discussions concerning the analysis and results. Liu Kuei-lin, Zhu Yu-cheng, and particularly Ye Sizong, of the People's Republic of China were in attendance during the data taking sessions, and we want to express our thanks for all the work that they did for us. The people in the HS Division at CERN provided us with whatever we asked for and have been supportive of this work from the beginning. We wish to particularly thank G. Bertuol and N. Aguilar for taking such an active interest in the experiment. Thanks are also due Donna Kubik (U. of W.) for emulsion scanning and measurements. Finally, the experiment could never have been done without full support from the leaders of the HS Division at CERN (A. Herz and K. Goebel), and the Radiation Physics Group at SLAC (R. C. McCall), and we are grateful to them for this.

REFERENCES

1. C. Richard-Serre, Evaluation de la perte d'énergie unitaire et du parcours pour des muons de 2 a 600 GeV dans un absorbant quelconque, CERN Report CERN-71-18 (September 1971).

2. W.R. Nelson, K.R. Kase and G.K. Svensson, Nucl. Instrum. Methods 120 (1974) 413.

3. D. Bintinger, J. Curry, J. Pilcher, C. Rubbia, L. Sulak, W. Ford, A.K. Mann, D. Cline, R. Imlay, and P. Wanderer, Phys. Rev. 35 (1975) 72.

4. K. Kobayakawa, Nuovo Cimento XLVII (1967) 156.

5. D. Keefe and C.M. Noble, Nucl. Instrum. Methods 64 (1968) 173.

6. R.G. Alsmiller,Jr., F.S. Alsmiller, J. Barish and Y. Shima, Muon Transport and the Shielding of High-Energy ($\leq$ 500 GeV) Proton Accelerators, Proc. Intern. Congr. on Protection Against Accelerator and Space Radiation (CERN Report Number CERN-71-16, Vol. 2 (1971) 601.

7. D. Theriot, M. Awschalom and K. Lee, Muon Shielding Calculations: Heterogeneous Passive and Active Shields, Applications to Experimental Beams and Areas, Proc. Intern. Congr. on Protection Against Accelerator and Space Radiation, CERN Report Number CERN-71-16, Vol. 2 (1971) 641.

8. M. Barbier and R. Hunter, Numbers and Spectrum of Muons from Proton-Induced Extranuclear Cascades in Shields, Proc. Intern. Congr. on Protection Against Accelerator and Space Radiation, CERN Report Number CERN-71-16, Vol. 2 (1971) 652.

9. E. Bertel and B. de Séréville, Un Programme de Calcul de Flux de Muons dans des Configurations Réelles, Proc. Intern. Congr. on Protection Against Accelerator and Space Radiation, CERN Report Number CERN-71-16, Vol 2 (1971) 678.

10. A. Van Ginneken, Penetration of Prompt and Decay Muon Components of Hadronic Cascades Through Thick Shields, Fermilab Report Number TM-630 (1975).

11. N.V. Mokhov, G.I. Semenova and A.V. Uzunian, Nucl. Instrum. Methods 180 (1981) 469.

12. W.R. Nelson, G.R. Stevenson, E.H.M. Heijne, P. Jarron, L. Kuei-lin and M. Nielsen, Preliminary Profile Measurements of High-Energy Muon Beams in a Soil Shield, CERN Report Number CERN/HS-RP/042 (1979).

13. W.R. Nelson, The Shielding of Muons Around High-Energy Electron Accelerators: Theory and Measurement, Ph.D. Dissertation in Health Physics and Dosimetry, Stanford University, 1973.

14. W.R. Nelson and K.R. Kase, Nucl. Instrum. Methods 120 (1974) 401.

15. L. Eyges, Phys. Rev. 74 (1948) 1534.

16. G.R. Stevenson, A Description of the TOMCAT Muon Transport Program, CERN Report Number HS-RP/IR/81-28(1981).

17. A. Van Ginneken, CASIM Program to Transport Hadronic Cascades in Bulk Matter, Fermilab Report Number FNAL-FN-272 (1975).

18. G.R. Stevenson, Possible Limits of Secondary Beam Intensities in the West Experimental Area Due to Radiation Exposure at the CERN Boundaries, CERN Report Number CERN LABII-RA/Note/74-14(1974).

19. H. Schonbacher, Calculation of Muon Dose Rates at the CERN Boundaries from Hadron Beams in the SPS West Experimental Area After Upgrading to 450 GeV, CERN Report Number HS-RP/TM/81-27 (1981).

20. E.H.M. Heijne, P. Jarron, P. Lazeyras, W.R. Nelson and G.R. Stevenson, IEEE Trans. Nucl. Sci. NS-27 (1980) 272.

21. E.H.M. Heijne, P. Jarron, T.M. Jenkins, W.R. Nelson, and H. Ing, Nucl. Instrum. Methods 205 (1983) 437.

22. R.L. Thompson, J.A. Kirk, M.E. Nelson, R.J. Piserchio, and J. Lord, Phys. Rev. 5 (1969) 177.

23. B. Rossi, High Energy Particles, Prentice Hall, Englewood Cliffs, N.J. (1952).

24. B. Rossi and K. Griesen, Rev. Mod. Phys. 13 (1941) 240.

25. H. Atherton, CERN, private communication.

TABLE I

Incident Momentum (GeV/c)	Integrated Fraction of Muons (Under Profile Curve)
280	1.22 ± 0.07
240	1.14 ± 0.05
200	0.33 ± 0.01
200 (no carbon)	0.88 ± 0.03
TOMCAT and TRANMU	1.0

TABLE II

Normalized Counts in Detectors (On Axis)*

Detector	A 41 Up / 62 Down	B 62 Up / 41 Down	A' 41 Up / 62 Down
S1	1000	1000	1000
S2	1019	1028	1009
S1•S2	802	798	831
41	1270	1011	1173
42	1250	1136	1180
61	1112	1160	999
62	1135	1195	1040
41•42•61	940	60	855
41/62 ratio	1.12	0.85	1.13

* For explanation see text.

FIGURE CAPTIONS

1. Mean range-energy curves for muons in various materials.
2. Plan view of the CERN experimental area.
3. Vertical section through the muon shield. Shaded area inside NA4 box represents 50 m carbon target.
4. Schematic view of location of scintillation counters in holes.
5. Sketch of support and slide system for telescopes and emulsions.
6. Flow diagram for scintillator electronics.
7. Metacryl plastic, coated on both sides with emulsion. The entry and exit points of tracks at the emulsion-plastic surfaces are represented as circles and squares, respectively. (X_t, Y_t) and (X_b, Y_b) are entry and exit points respectively of tracks at the metacryl surfaces used for determining beam direction. $(X_t, Y_t)_i$ and $(X_b, Y_b)_i$ are entry and exit points respectively for other tracks used to determine angular information.
8. Si diode telescope arrangement.
9. Comparison between TOMCAT (solid line) and TRANMU (histogram): Radial distribution for 280 GeV/c incident muons (with carbon target).
10. Comparison between TOMCAT (solid line) and TRANMU (histogram): Radial distribution for 240 GeV/c incident muons (with carbon target).
11. Comparison between TOMCAT (solid line) and TRANMU (histogram): Radial distribution for 200 GeV/c incident muons (with carbon target).
12. Comparison between TOMCAT (solid line) and TRANMU (histogram): Radial distribution for 200 GeV/c incident muons (without carbon target).
13. Scintillation counter data for 280 GeV/c incident muons. Reference counters R1 and R2 are denoted by plus and asterisk symbols, respectively. Data taken in Hole 1 are denoted by circles, and in Hole 2 by squares. Open symbols represent counter CA and closed counter CB.
14. Scintillation counter data for 240 GeV/c incident muons.
15. Scintillation counter data for 200 GeV/c incident muons.

16. Scintillation counter data for 200 GeV/c incident muons with the 50 m carbon target removed.

17. Comparison of measured angular distribution with TRANMU calculation near the beam centerline in Hole 1 for 280 GeV/c incident muons.

18. Fluences measured by emulsion compared with scintillator data (shaded band) and TOMCAT (solid line) for 280 GeV/c incident muons.

19. Fluences measured by emulsion compared with scintillator data (shaded band) and TOMCAT (solid line) for 240 GeV/c incident muons.

20. Fluences measured by emulsion compared with scintillator data (shaded band) and TOMCAT (solid line) for 200 GeV/c incident muons.

21. Fluences measured by the Si diode compared with scintillator data (shaded band) and TOMCAT (solid line) for 280 GeV/c incident muons.

22. Fluences measured with scintillators fixed in the holes, and the current in magnet B9 varied. Data have been normalized to the same scale as previous runs (i.e., relative vertical distance). The shaded band represents the previous scintillator data (see fig. 15).

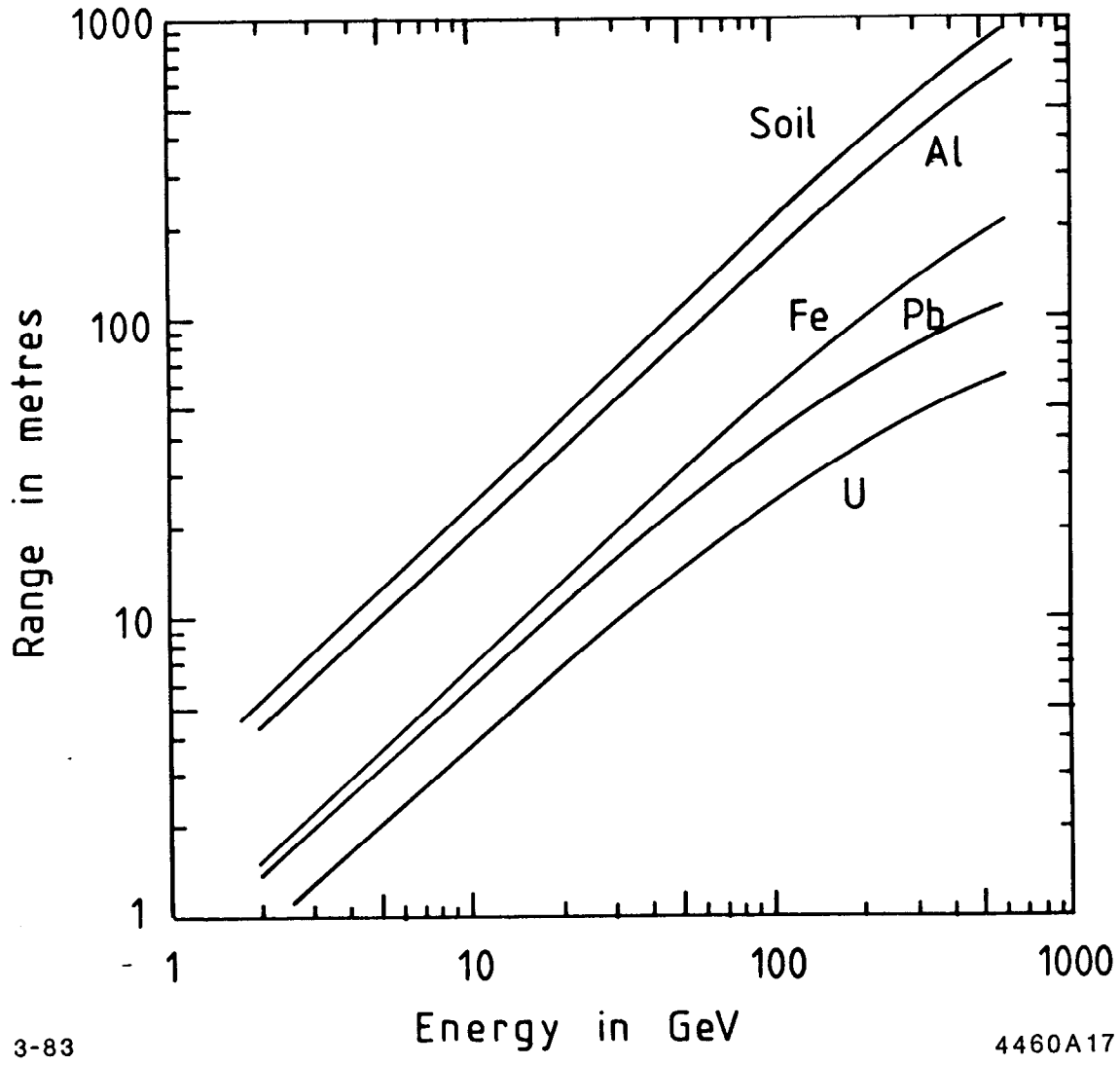
1000
100
10
1
Range in metres
Soil
Al
Fe
Pb
U
1
10
100
1000
Energy in GeV
3-83
4460A17

Fig. 1

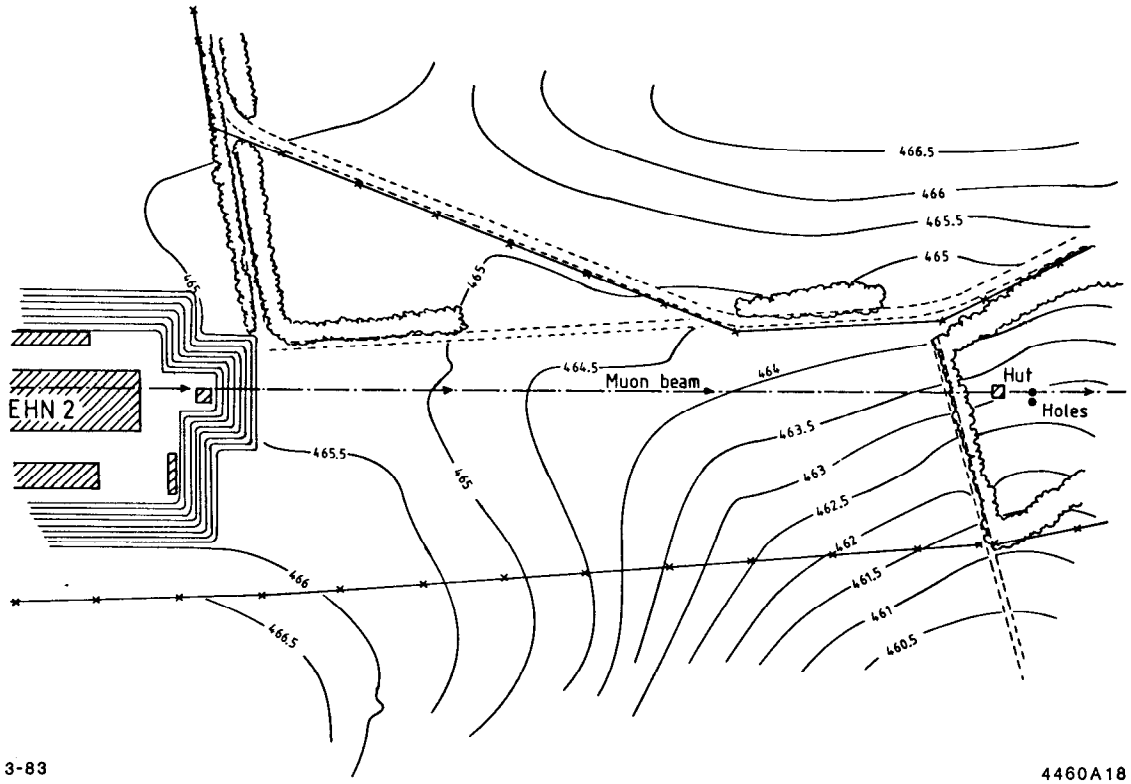
466.5
466
465.5
465
464.5
Muon beam
464
Hut
Holes
EHN 2
463.5
463
462.5
462
461.5
461
460.5
465.5
466
466.5
3-83
4460A18

Fig. 2

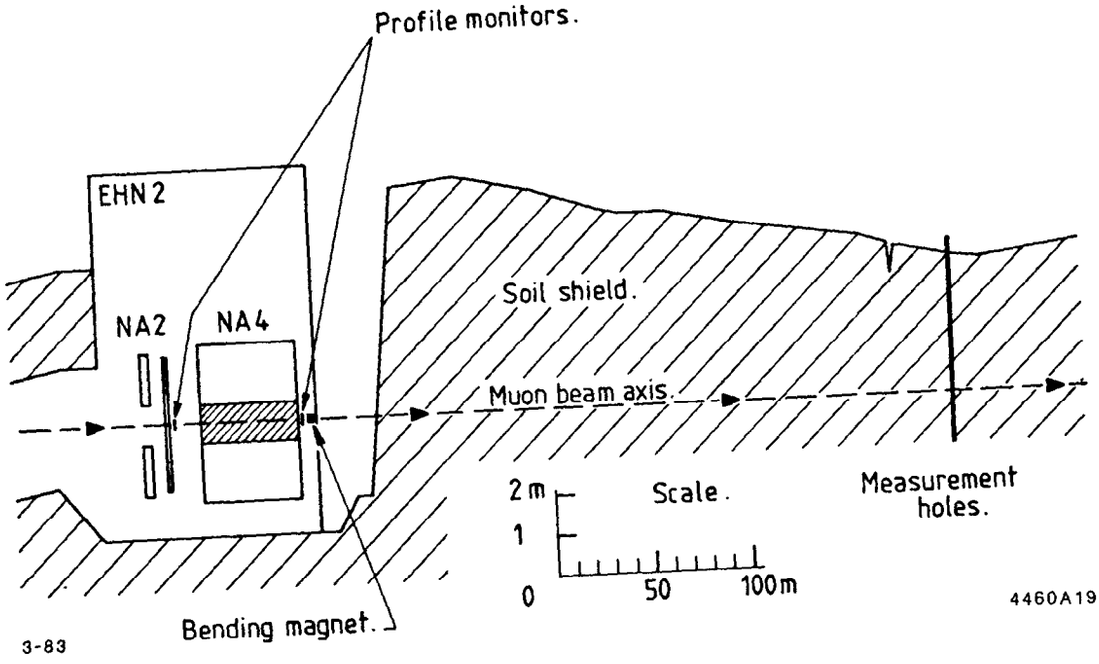
Profile monitors.
EHN 2
NA2
NA4
Soil shield.
Muon beam axis.
2 m
1
0
Scale.
50
100 m
Measurement holes.
4460A19
3-83
Bending magnet.

Fig. 3

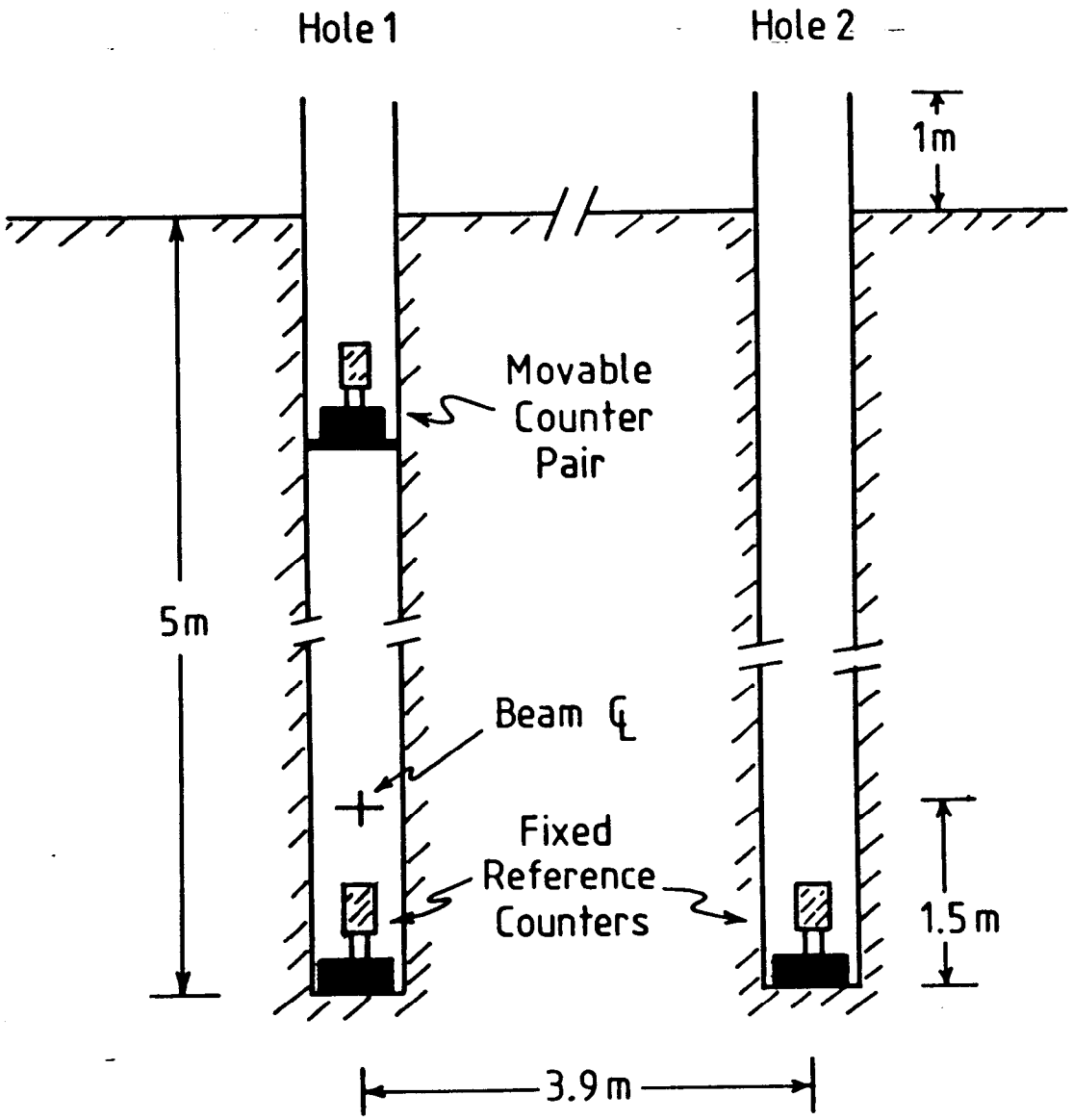

3-83

View from Beam Direction

4460A20

Fig. 4

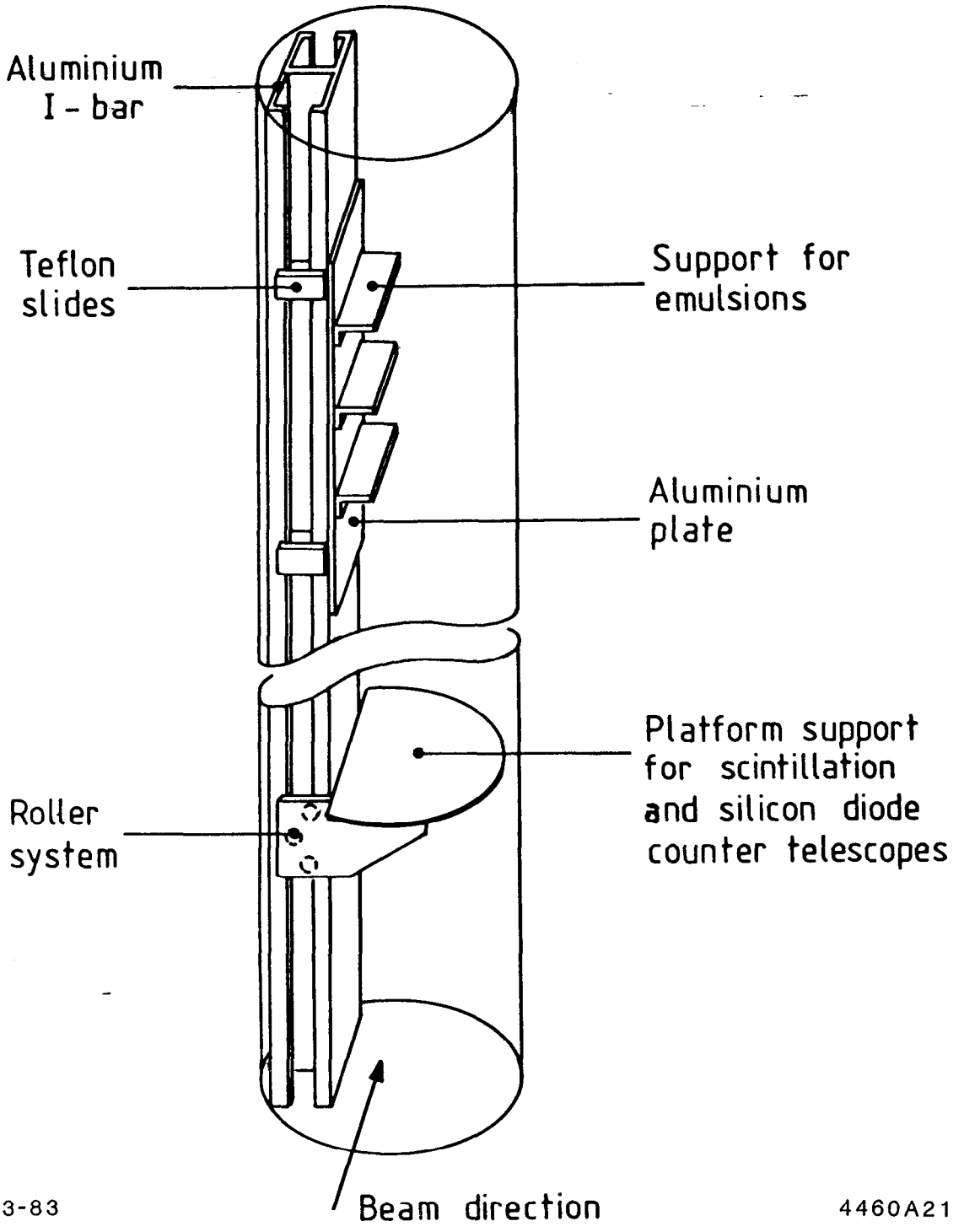
Aluminium
I - bar
Teflon
slides
Support for
emulsions
Aluminium
plate
Platform support
for scintillation
and silicon diode
counter telescopes
Roller
system
Beam direction
3-83
4460A21

Fig. 5

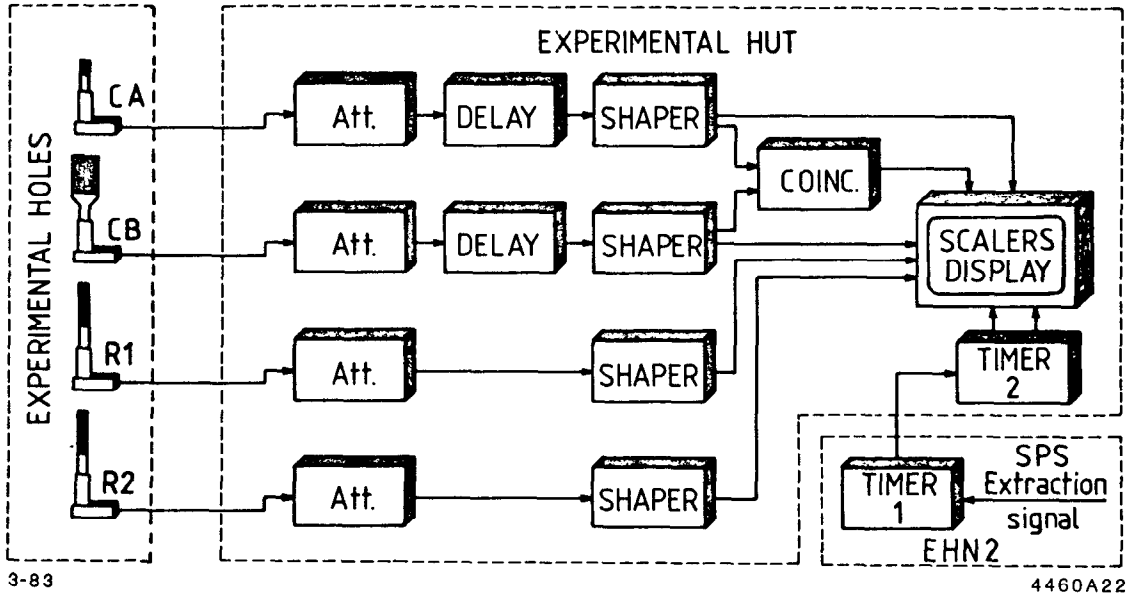
EXPERIMENTAL HUT
EXPERIMENTAL HOLES
CA
CB
R1
R2
Att.
Att.
Att.
Att.
DELAY
DELAY
SHAPER
SHAPER
SHAPER
SHAPER
COINC.
SCALERS DISPLAY
TIMER 2
TIMER 1
SPS Extraction signal
EHN2
3-83
4460A22

Fig. 6

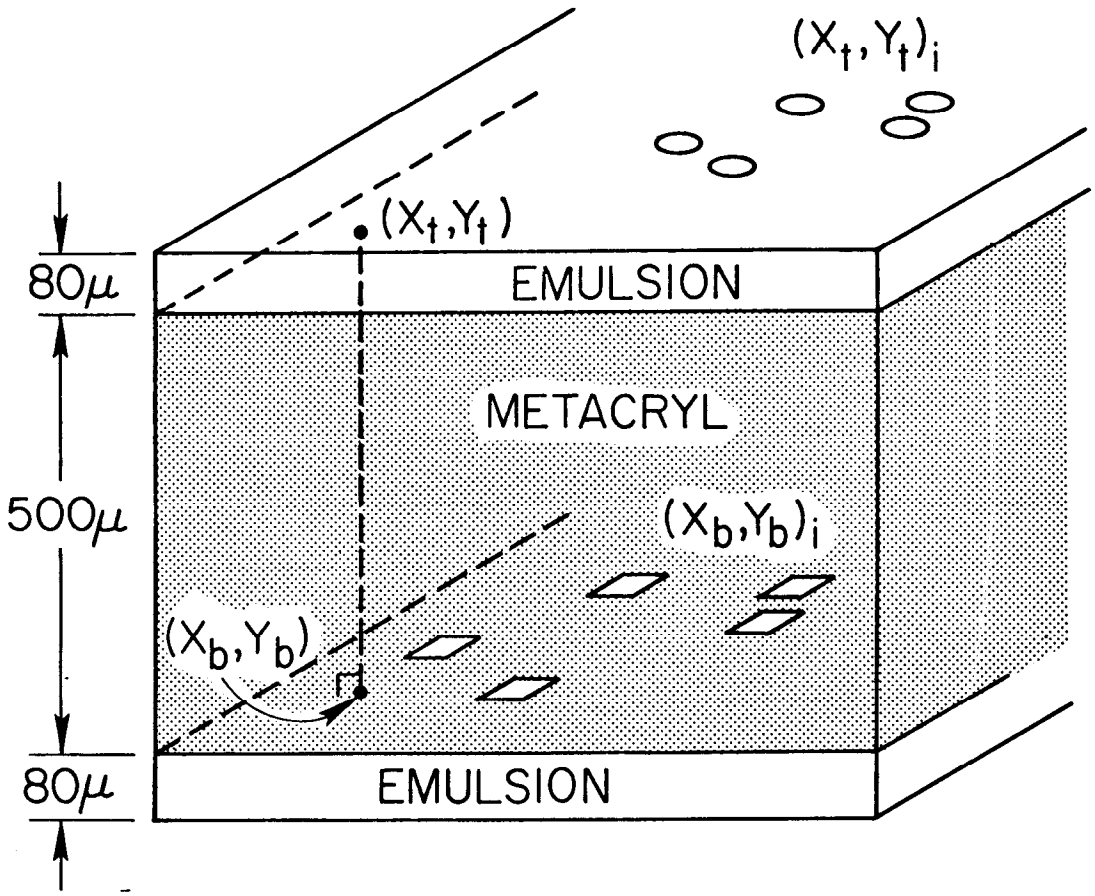

2-83

4460A1

Fig. 7

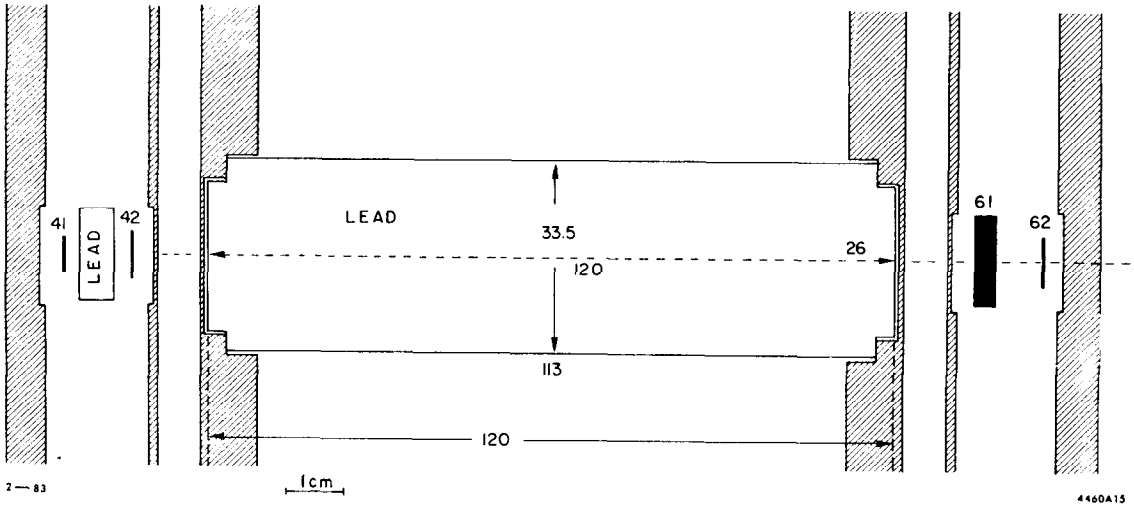

Fig. 8

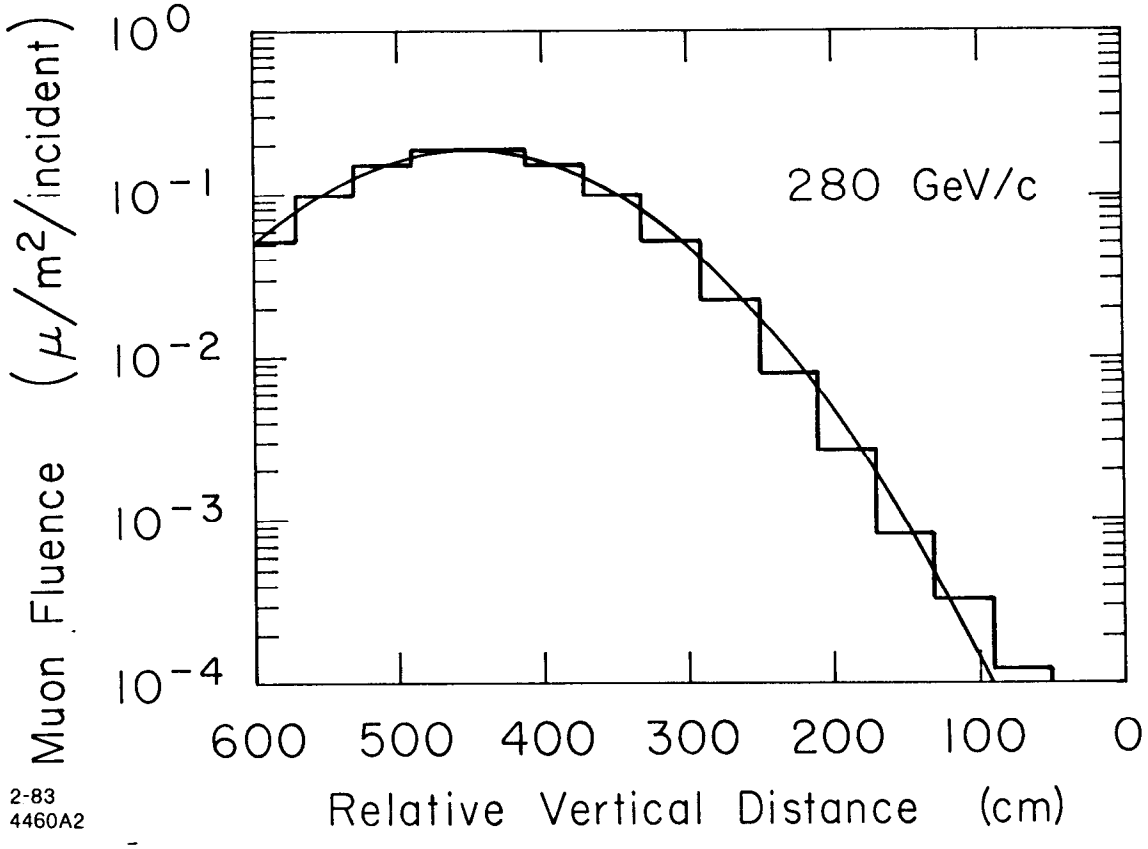
Muon Fluence (μ/m²/incident)
10⁰
10⁻¹
10⁻²
10⁻³
10⁻⁴
280 GeV/c
600 500 400 300 200 100 0
Relative Vertical Distance (cm)
2-83
4460A2

Fig. 9

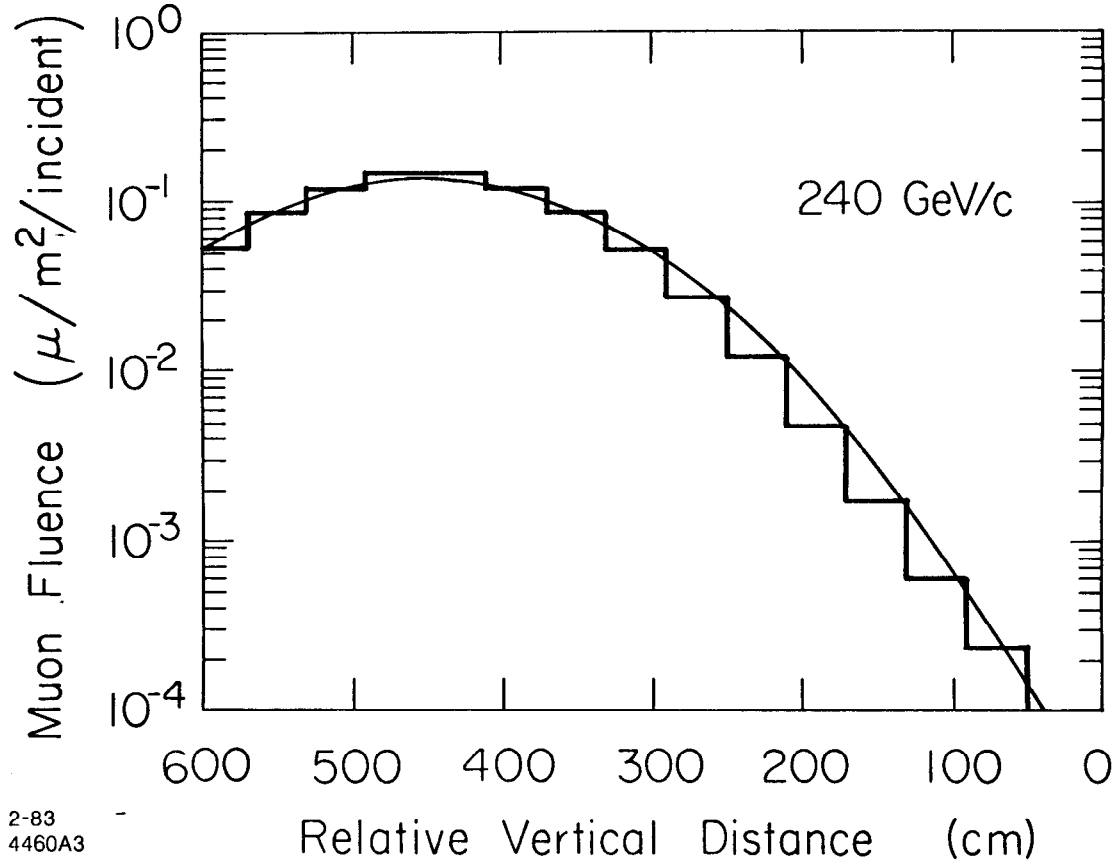
Muon Fluence (μ/m²/incident)
10⁰
10⁻¹
10⁻²
10⁻³
10⁻⁴
240 GeV/c
600
500
400
300
200
100
0
Relative Vertical Distance (cm)
2-83
4460A3

Fig. 10

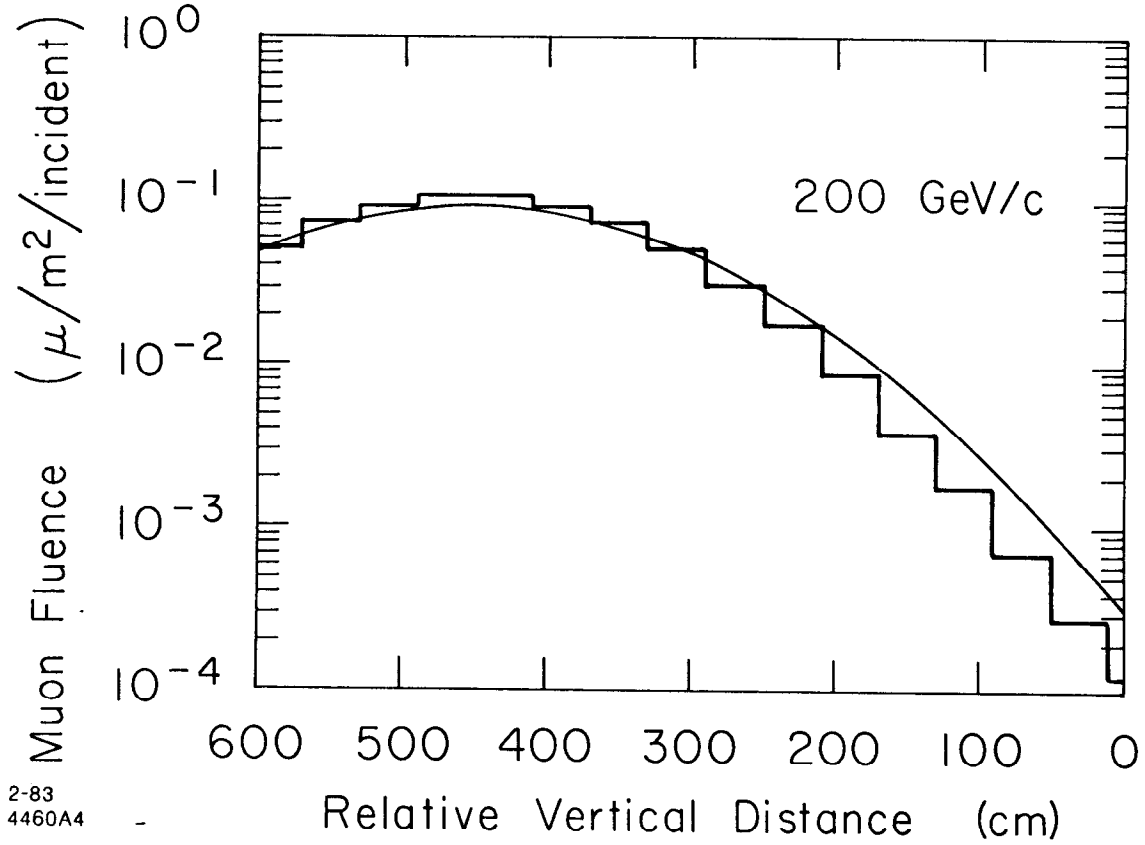
Muon Fluence (μ/m²/incident)
10⁰
10⁻¹
10⁻²
10⁻³
10⁻⁴
200 GeV/c
600 500 400 300 200 100 0
Relative Vertical Distance (cm)
2-83
4460A4

Fig. 11

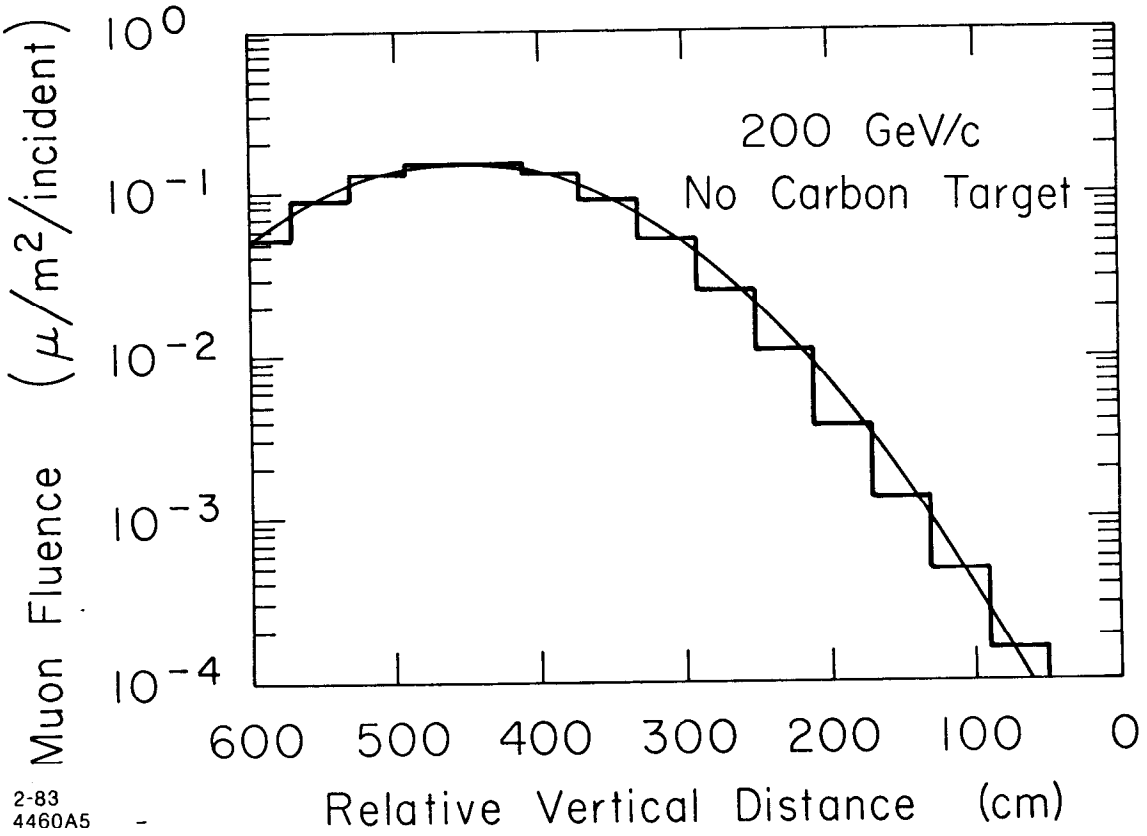
Muon Fluence (μ/m²/incident)
10⁰
10⁻¹
10⁻²
10⁻³
10⁻⁴
200 GeV/c
No Carbon Target
600 500 400 300 200 100 0
Relative Vertical Distance (cm)
2-83
4460A5

Fig. 12

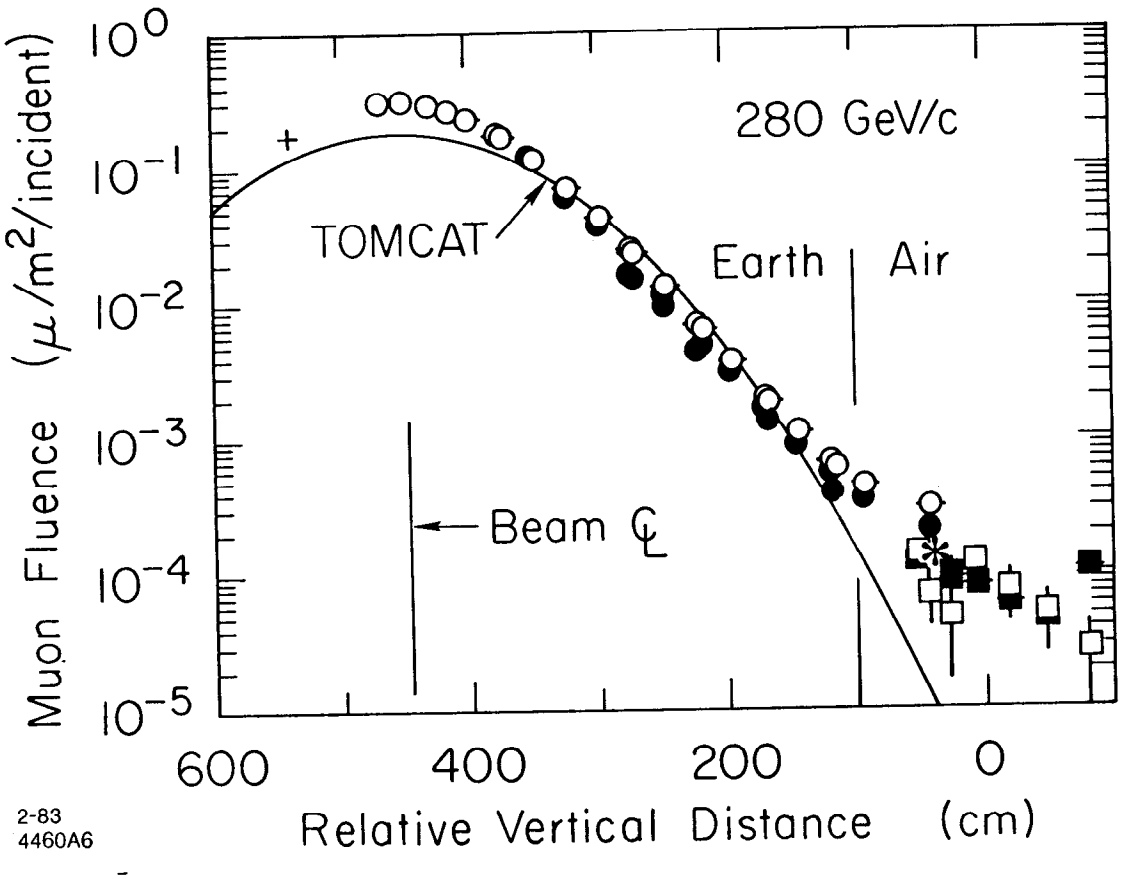
Muon Fluence (μ/m^2/incident)
10^0
10^{-1}
10^{-2}
10^{-3}
10^{-4}
10^{-5}
280 GeV/c
TOMCAT
Earth
Air
Beam ℄
600
400
200
0
Relative Vertical Distance (cm)
2-83
4460A6

Fig. 13

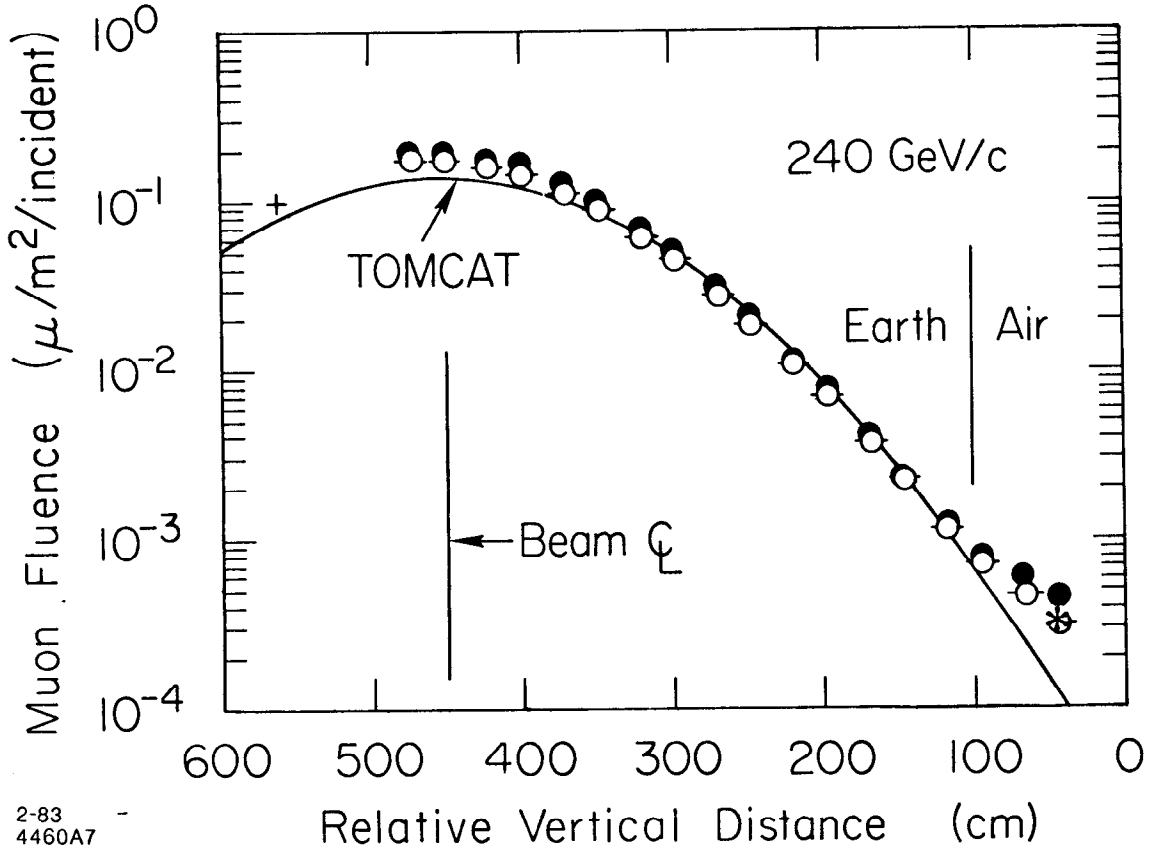
Muon Fluence (μ/m^2/incident)
10^0
10^{-1}
10^{-2}
10^{-3}
10^{-4}
240 GeV/c
TOMCAT
Earth
Air
Beam ℄
600
500
400
300
200
100
0
Relative Vertical Distance (cm)
2-83
4460A7

Fig. 14

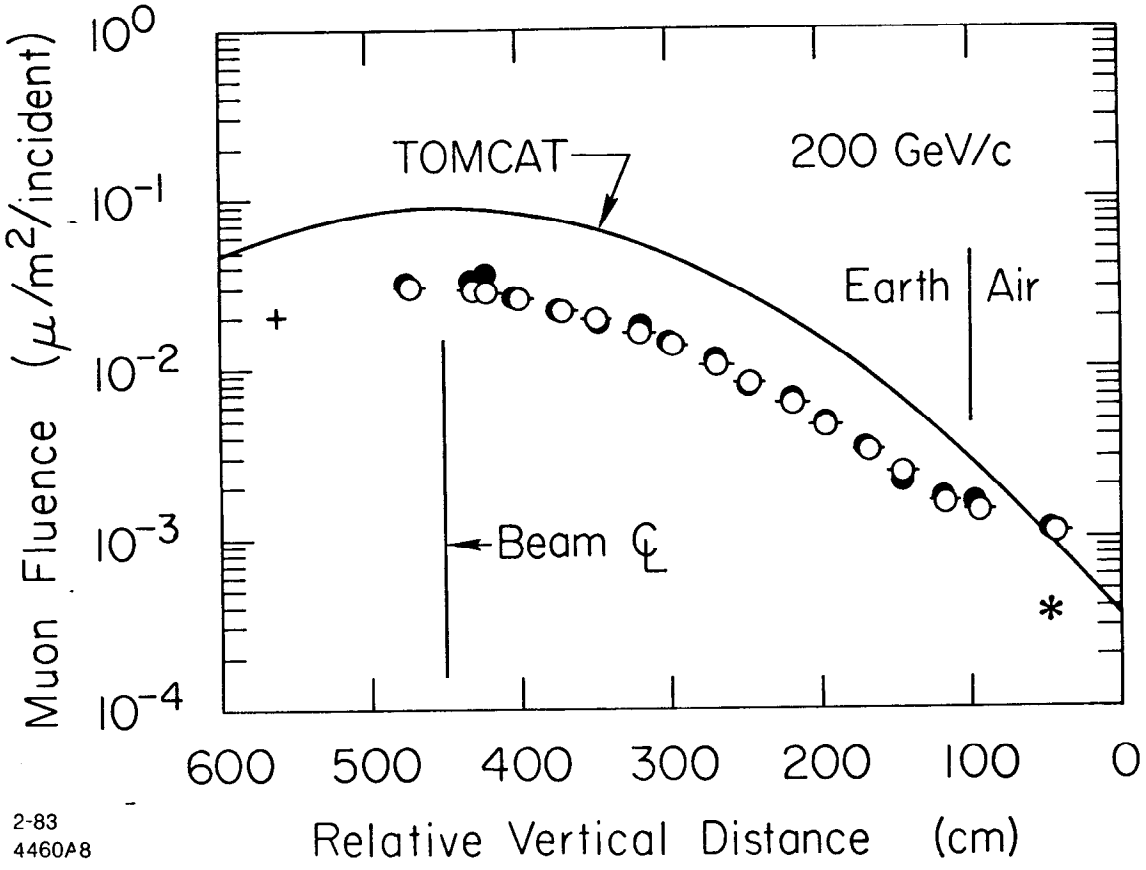
Muon Fluence (μ/m²/incident)
10⁰
10⁻¹
10⁻²
10⁻³
10⁻⁴
TOMCAT
200 GeV/c
Earth
Air
Beam ℄
600
500
400
300
200
100
0
Relative Vertical Distance (cm)
2-83
4460A8

Fig. 15

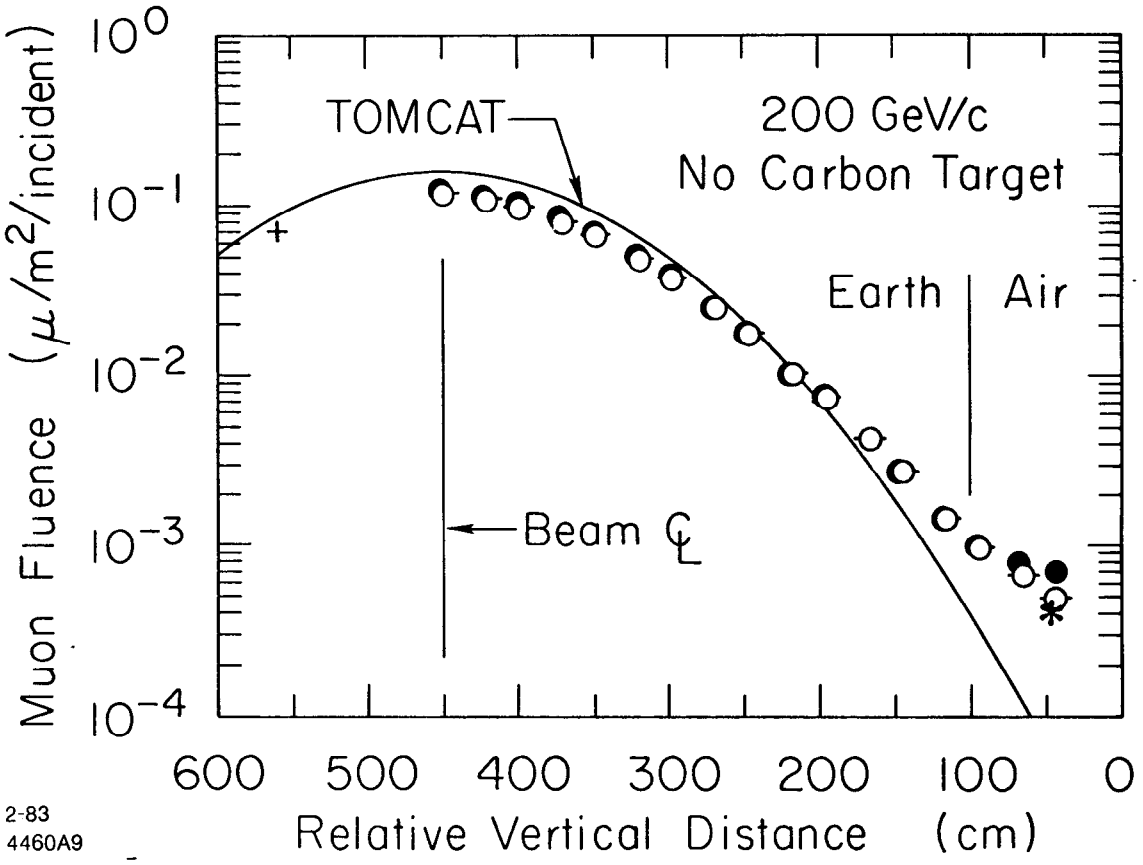
TOMCAT
200 GeV/c
No Carbon Target
Earth
Air
Beam ℄
Muon Fluence (μ/m²/incident)
10⁰
10⁻¹
10⁻²
10⁻³
10⁻⁴
600
500
400
300
200
100
0
Relative Vertical Distance (cm)
2-83
4460A9

Fig. 16

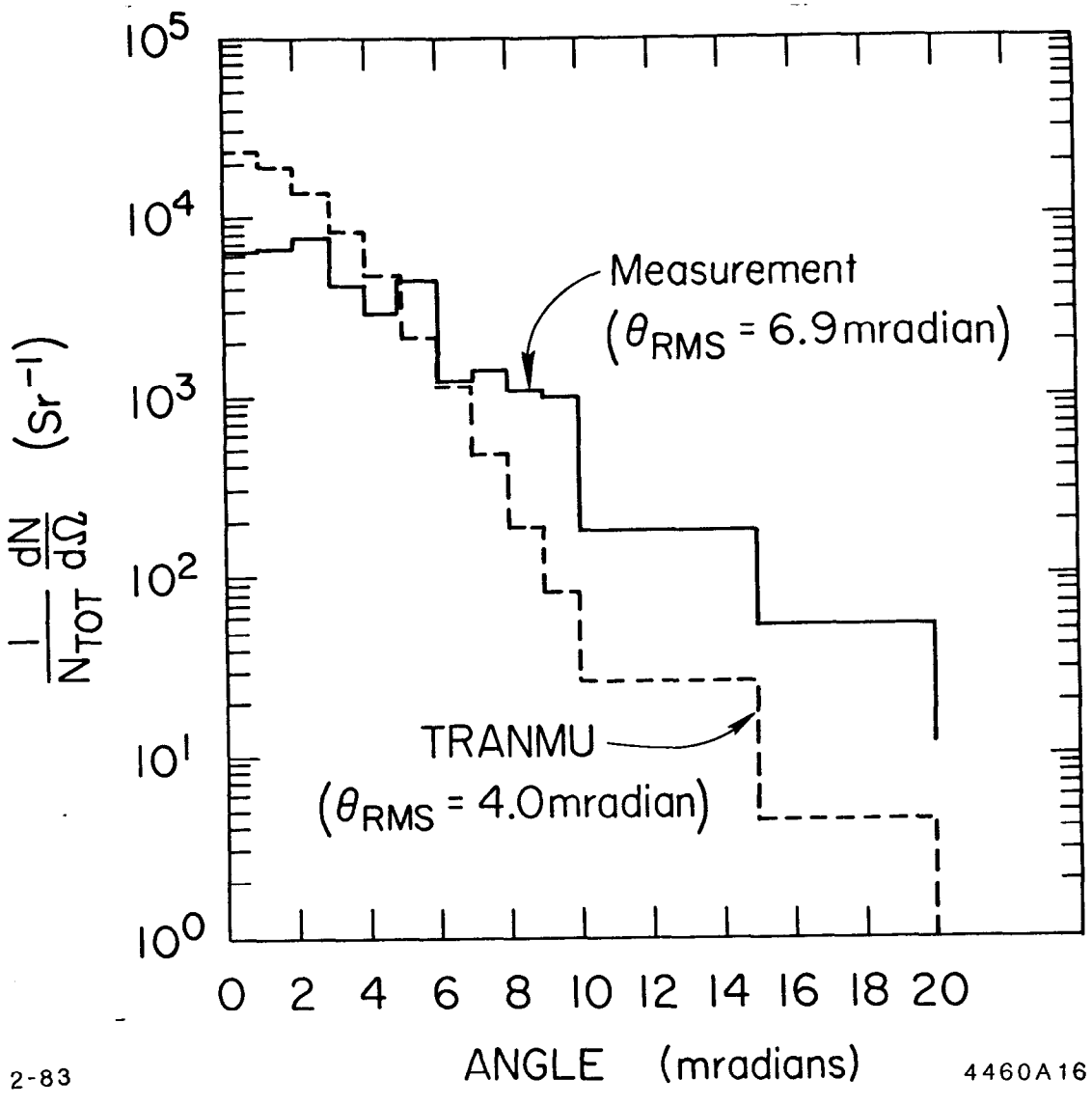
10^5
10^4
10^3
10^2
10^1
10^0
$\frac{1}{N_{TOT}} \frac{dN}{d\Omega}$ (Sr^{-1})
Measurement
(θ_{RMS} = 6.9mradian)
TRANMU
(θ_{RMS} = 4.0mradian)
0 2 4 6 8 10 12 14 16 18 20
ANGLE (mradians)
2-83
4460A16

Fig. 17

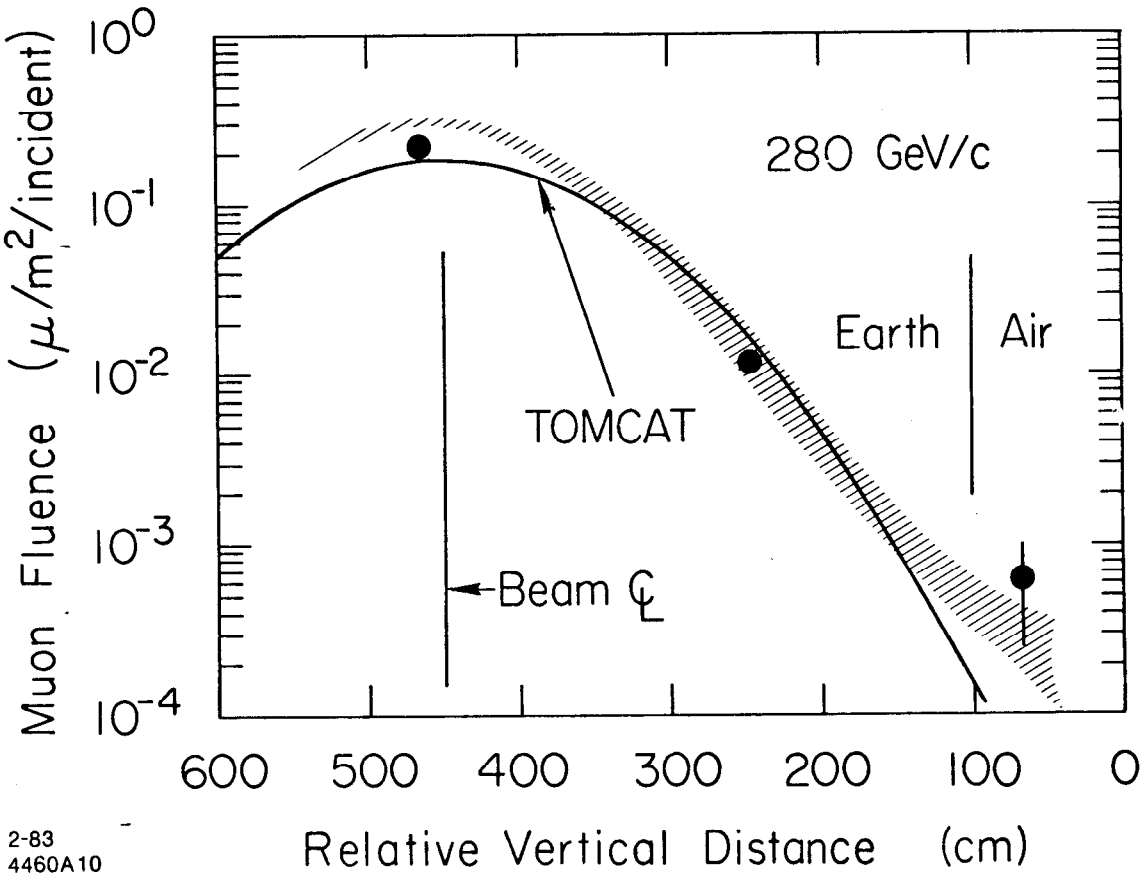
Muon Fluence (μ/m^2/incident)
10^0
10^{-1}
10^{-2}
10^{-3}
10^{-4}
280 GeV/c
Earth
Air
TOMCAT
Beam ℄
600
500
400
300
200
100
0
Relative Vertical Distance (cm)
2-83
4460A10

Fig. 18

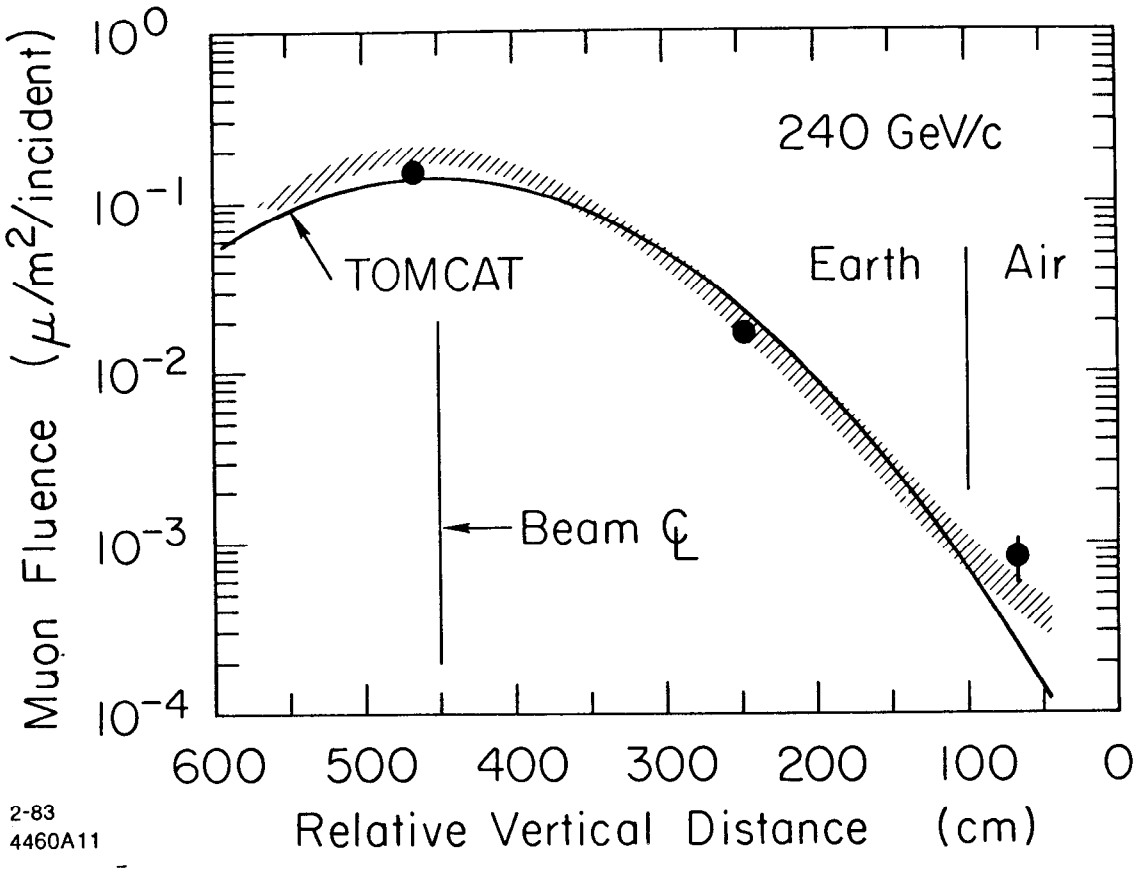
240 GeV/c
TOMCAT
Earth
Air
Beam ℄
Muon Fluence (μ/m²/incident)
10⁰
10⁻¹
10⁻²
10⁻³
10⁻⁴
600
500
400
300
200
100
0
Relative Vertical Distance (cm)
2-83
4460A11

Fig. 19

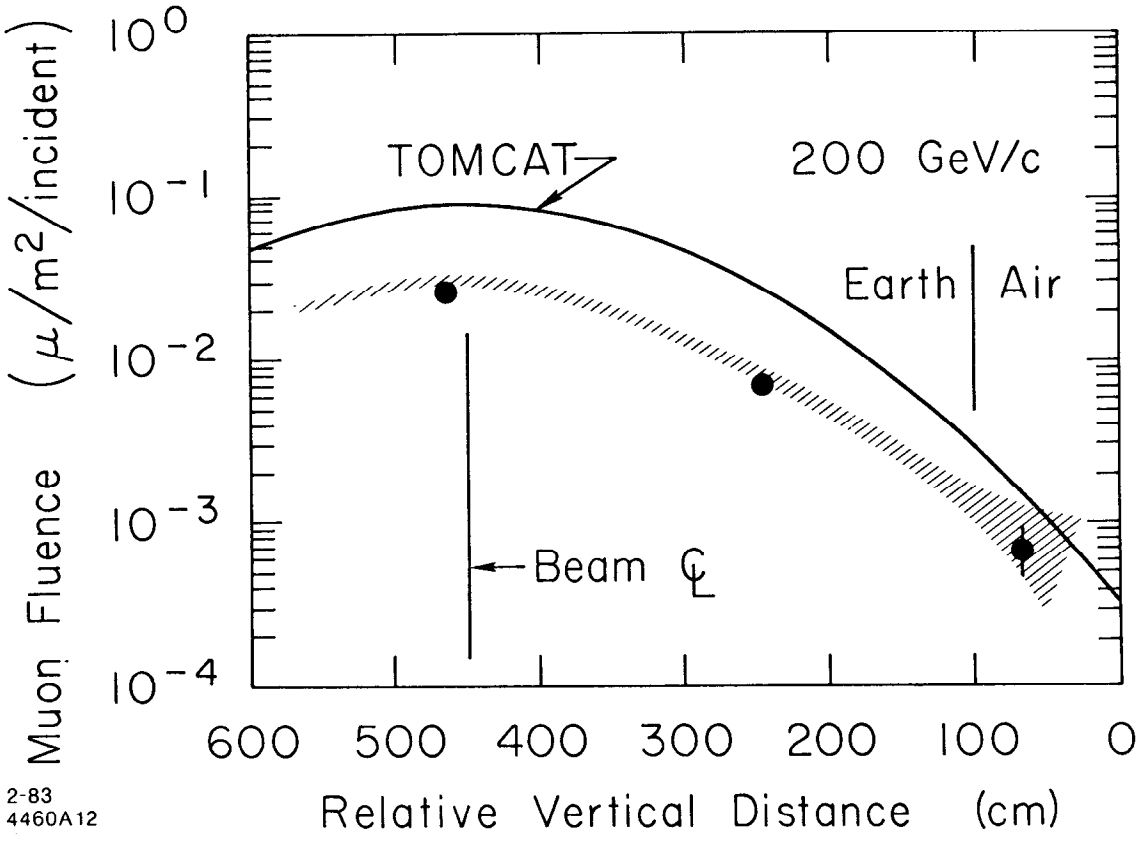
Muon Fluence (μ/m²/incident)
10⁰
10⁻¹
10⁻²
10⁻³
10⁻⁴
TOMCAT
200 GeV/c
Earth
Air
Beam ℄
600
500
400
300
200
100
0
Relative Vertical Distance (cm)
2-83
4460A12

Fig. 20

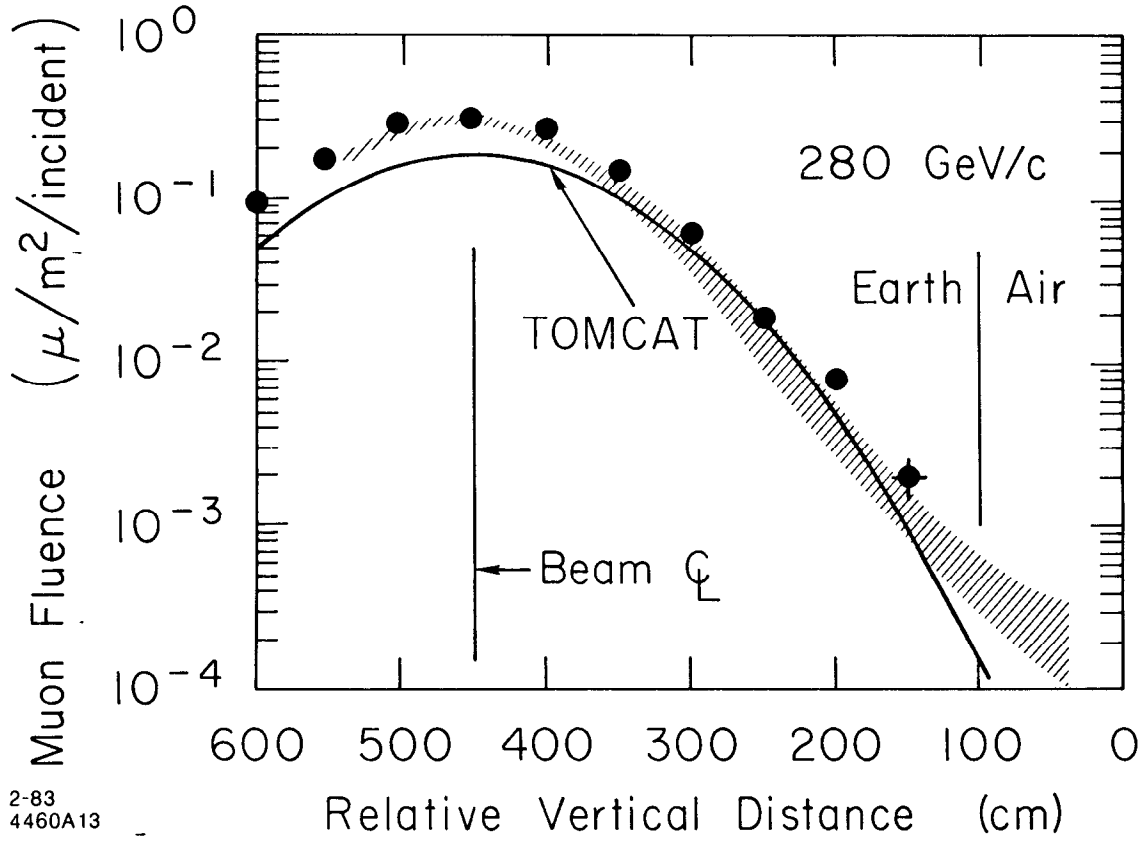
Muon Fluence (μ/m²/incident)
10⁰
10⁻¹
10⁻²
10⁻³
10⁻⁴
280 GeV/c
Earth
Air
TOMCAT
Beam ℄
600
500
400
300
200
100
0
Relative Vertical Distance (cm)
2-83
4460A13

Fig. 21

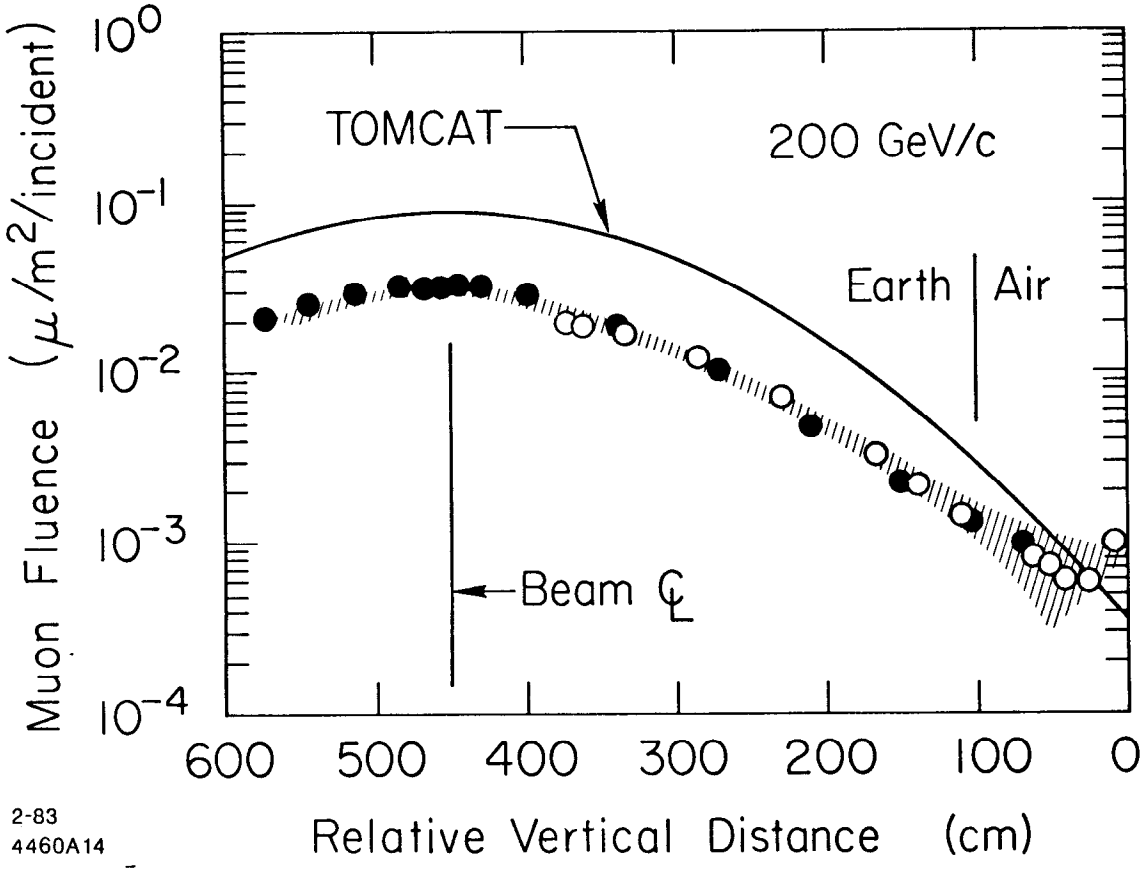
TOMCAT
200 GeV/c
Earth
Air
Beam ℄
Muon Fluence (μ/m²/incident)
10⁰
10⁻¹
10⁻²
10⁻³
10⁻⁴
600
500
400
300
200
100
0
Relative Vertical Distance (cm)
2-83
4460A14

Fig. 22